Y.H.Bian, C.Zhang

THERMAL-MAGNETIC-ELASTIC EFFECT ANALYSIS OF A THIN CURRENT-CARRYING CONICAL FRUSTUM SHELL

Key Laboratory of Mechanical Reliability for Heavy Equipments and Large Structures of Hebei Province, College of Civil Engineering and Mechanics, Yanshan University, Qinhuangdao, China; e-mail: yh_bian@sina.com

Abstract. A thermal-magnetic-elastic problem for a thin current-carrying conical frustum shell in a magnetic field is studied. The normal Cauchy form of nonlinear differential equations, which include in total eight basic unknown variables, are obtained by the variable replacement method. Using the Newmark's stable finite equidifferent formulas and the quasi-linearization method, the nonlinear partial differential equations are reduced to a sequence of quasi-linear differential equations, which can be solved by the discrete-orthogonalization method. The temperature field in a thin conical frustum shell and the integral eigenvalues are derived after considering Joule's heat effect in an electromagnetic field and the thermal equilibrium equation. The change of stresses, displacements, and temperatures in the thin current-carrying conical frustum shell with variation of the electromagnetic parameters is discussed. It is proved that the stresses, strains, and temperatures in thin shells can be controlled by changing the electromagnetic and mechanical parameters by considering a specific example. These results are expected to be a theoretical reference for further analysis of this case.

Key words: thermal-magnetic-elasticity, thin conical frustum shell, coupling effect, Lorentz force, quasi-linearization method, discrete-orthogonalization method.

1. Introduction.

Applications of electromagnetic elastic structures are broad in modern technological fields, such as aerospace industry, electromagnetic emission, power supply equipment, magnetoacoustic processing, etc. The objects moving in the applied magnetic field will come under the interaction of an electromagnetic field, a temperature field, and a mechanical field. The more complex mechanics behaviors have been shown, and the operations of the system are influenced. Therefore, the researches on the thermal-magnetic-elastic problem have both theoretically and practically important significance. In recent years, electromagnetic elastic mechanics has developed very quickly. Many important achievements have been obtained, such as Pao and Yeh [1] (1973); Ambartsumyan [2] (1977); Moon [3] (1984); Van de Ven [4] (1986); Ulitko, Mol'chenko, Kovalchuk [5] (1994); Mol'chenko, Grigorenko [6] (2010); Mol'chenko [7 – 12] (1989, 2012, 2013, 2014, 2015, 2016); Bian [13] (2015); Zheng, Zhang, Zhou [14] (2005); Qin [15, 16] (2003, 2009); Pratiher [17] (2011); Ootao, Ishihara [18] (2013); Kuang [19] (2014); Soni, Jain, Joshi [20] (2017); Mohammadimehr, Rostami [21] (2018), and others. These research achievements laid a good foundation for studies on electromagnetic elastic mechanics and its applications. However, these researches fasten mostly on the problems about the vibration and stability of magnetoelastic bodies, studies on magnetoelastic stress-strain problems of current-carrying plates and shells, especially, studies on a thermal-magnetic-elastic problem with considering temperature fields have rarely been seen. Therefore, the thermal-magnetic-elastic stress-strain analysis for current-carrying plates and shells is recently one of the interested topics studied.

In this paper, a thermal-magnetic-elastic problem for a thin current-carrying conical frustum shell in a magnetic field is studied. Based on the nonlinear magnetoelastic kinetic equations, geometric equations, physical equations, and electrodynamics equations of a thin shell under the interaction of an electromagnetic field, a temperature field, and a mechanical field, the fundamental equations for the nonlinear stress-strain problem under the action of the coupling field are given. The temperature field in a thin conical frustum shell and the integral eigenvalues are derived after considering Joule's heat effect in an electromagnetic field and the thermal equilibrium equation. The stresses, displacements, and temperatures of the thin conical frustum shell in a magnetic field are computed. The effect of the side current, electromagnetic induction density, etc. on the stresses, displacements, and temperatures in the thin conical frustum shell is analyzed.

2. Fundamental Equations.

Under the precondition of symmetrical loads, the thin conical frustum shell can be regarded axisymmetric. An orthogonal curvilinear coordinate system s, θ, ζ is shown in Fig. 1. By satisfying the magnetoelastic supposition of the thin shell [7] and using elastic mechanics theories, Ohm's law and Maxwell equations in electromagnetic basic theories, the fundamental equations for the thin conical frustum shell can be derived as follows:

The magnetoelastic kinetic equations are given by

$$\frac{\partial(rN_s)}{\partial s} - \cos\varphi N_\theta + r(F_s + \rho f_s) = r\rho h \frac{\partial^2 u}{\partial t^2}; \tag{1}$$

$$\frac{\partial(rQ_s)}{\partial s} - \sin\varphi N_\theta + r(F_\zeta + \rho f_\zeta) = r\rho h \frac{\partial^2 w}{\partial t^2}; \tag{2}$$

$$\frac{\partial(rM_s)}{\partial s} - \cos\varphi M_\theta - r\left(N_s - \frac{\sin\varphi}{r} M_\theta\right)\theta_s - rQ_s = \frac{r\rho h^3}{12} \cdot \frac{\partial^2 \theta_s}{\partial t^2}. \tag{3}$$

The electrodynamics equations are given by

$$-\frac{\partial B_\zeta}{\partial t} = \frac{1}{r} \cdot \frac{\partial(rE_\theta)}{\partial s}; \tag{4}$$

$$\sigma\mu\left[E_\theta + \frac{1}{2}\frac{\partial w}{\partial t}(B_s^+ + B_s^-) - \frac{\partial u}{\partial t} B_\zeta\right] = -\frac{\partial B_\zeta}{\partial s} + \frac{B_s^+ - B_s^-}{rh}. \tag{5}$$

The relations between the displacements and the strains are given by

$$\varepsilon_s = \frac{\partial u}{\partial s} + \frac{1}{2}\theta_s^2; \quad \varepsilon_\theta = \frac{u}{r}\cos\varphi + \frac{w}{r}\sin\varphi; \tag{6a, b}$$

$$\kappa_s = \frac{\partial \theta_s}{\partial s}; \quad \kappa_\theta = \frac{\cos\varphi}{r}\theta_s; \quad \theta_s = -\frac{\partial w}{\partial s}. \tag{7a, b, c}$$

The relations between the internal forces and the strains are given by

$$N_s = D_N[\varepsilon_s + \nu\varepsilon_\theta - (1+\nu)\varepsilon_T]; \quad N_\theta = D_N[\varepsilon_\theta + \nu\varepsilon_s - (1+\nu)\varepsilon_T]; \tag{8a, b}$$

$$M_s = D_M[\kappa_s + \nu\kappa_\theta - (1+\nu)\kappa_T]; \quad M_\theta = D_M[\kappa_\theta + \nu\kappa_s - (1+\nu)\kappa_T], \tag{9a, b}$$

where σ is the electrical conductivity of the material; μ is the permeability of the material; h is the thickness of the thin shell; t is the time variable; r is the radius of the section round; φ is the angle between the normal of the neutral surface and the rotation axis; B_s^+

and B_s^- are the values of B_s on the outer and inner surfaces of the thin conical frustum shell, respectively; ε_s and ε_θ are the strains in the corresponding directions; κ_s and κ_θ are the bending strains; u, w, and θ_s are the displacements and the angle of rotation in the corresponding directions; E_θ is the electric field intensity in the θ-direction; B_ζ is the magnetic induction intensity in the ζ-direction; F_s and F_ζ are the surface forces in the corresponding directions on the thin shell; ρf_s and ρf_ζ are the Lorentz forces in the corresponding directions; ρ is the mass density of the medium; N_s, N_θ, Q_s, M_s, and M_θ are the internal forces and moments in the corresponding directions in the thin conical frustum shell; $D_N(=Eh/(1-\nu^2))$ and $D_M(=Eh^3/[12(1-\nu^2)])$ are the tensile and bending rigidities of the thin conical frustum shell, respectively; E is elastic modulus; ν is Poisson's ratio; ε_T and κ_T are the integral eigenvalues of the temperature field T along the thickness of the thin conical frustum shell, that is

$$\varepsilon_T = \frac{1}{h}\int_{-h/2}^{h/2} \alpha_T T(s,\theta,\zeta,t)\mathrm{d}\zeta\ ;\ \kappa_T = \frac{12}{h^3}\int_{-h/2}^{h/2} \alpha_T T(s,\theta,\zeta,t)\zeta\,\mathrm{d}\zeta\ , \tag{10a, b}$$

where α_T is the linear expansion coefficient of the material; $T(s,\theta,\zeta,t)$ is the temperature distributing function in the thin shell.

For obtaining normal Cauchy form nonlinear partial differential equations, let u, w, θ_s, N_s, Q_s, M_s, B_ζ, and E_θ be the basic unknown variables. We obtain:

$$\frac{\partial u}{\partial s} = \frac{(1-\nu^2)}{Eh}N_s - \frac{\nu\sin\varphi}{r}w - \frac{\nu\cos\varphi}{r}u - \frac{1}{2}\theta_s^2 + (1+\nu)\varepsilon_T; \tag{11}$$

$$\frac{\partial w}{\partial s} = -\theta_s; \tag{12}$$

$$\frac{\partial \theta_s}{\partial s} = \frac{12(1-\nu^2)}{Eh^3}M_s - \frac{\nu\cos\varphi}{r}\theta_s + (1+\nu)\kappa_T; \tag{13}$$

$$\frac{\partial N_s}{\partial s} = \frac{\cos\varphi}{r}\left[(\nu-1)N_s + Eh\left(\frac{\cos\varphi}{r}u + \frac{\sin\varphi}{r}w\right)\right] - Eh\frac{\cos\varphi}{r}\varepsilon_T - (F_s + \rho f_s) + \rho h\frac{\partial^2 u}{\partial t^2}; \tag{14}$$

$$\frac{\partial Q_s}{\partial s} = \frac{\sin\varphi}{r}\left[\nu N_s + Eh\left(\frac{\cos\varphi}{r}u + \frac{\sin\varphi}{r}w\right) - Eh\varepsilon_T\right] - \frac{\cos\varphi}{r}Q_s - (F_\zeta + \rho f_\zeta) + \rho h\frac{\partial^2 w}{\partial t^2}; \tag{15}$$

$$\frac{\partial M_s}{\partial s} = \frac{\cos\varphi}{r}\left[(\nu-1)M_s + \frac{Eh^3}{12}\left(\frac{\cos\varphi}{r}\theta_s - \kappa_T\right)\right] - \frac{\sin\varphi}{r}\left[\nu M_s + \frac{Eh^3}{12}\left(\frac{\cos\varphi}{r}\theta_s - \kappa_T\right)\right]\theta_s +$$

$$+ N_s\theta_s + Q_s + \frac{\rho h^3}{12}\cdot\frac{\partial^2\theta_s}{\partial t^2}; \tag{16}$$

$$\frac{\partial B_\zeta}{\partial s} = -\sigma\mu\left[E_\theta + \frac{1}{2}(B_s^+ + B_s^-)\frac{\partial w}{\partial t} - B_\zeta\frac{\partial u}{\partial t}\right] + \frac{B_s^+ - B_s^-}{rh}; \tag{17}$$

$$\frac{\partial E_\theta}{\partial s} = -\frac{\partial B_\zeta}{\partial t} - \frac{\cos\varphi}{r}E_\theta. \tag{18}$$

3. Computational Method.

Equations (11) – (18) can be written as boundary-value problems:

$$\frac{\partial \mathbf{N}}{\partial s} = \mathbf{F}(s, \mathbf{N}) \quad (s_0 \le s \le s_N); \tag{19}$$

$$D_1\mathbf{N}(s_0) = \mathbf{d}_1; \quad D_2\mathbf{N}(s_N) = \mathbf{d}_2, \tag{20a, b}$$

where $\mathbf{N} = \{u, w, \theta_s, N_s, Q_s, M_s, B_\zeta, E_\theta\}^{\mathrm{T}}$ is eight-dimensional vector; D_1 and D_2 are given orthogonal matrixes that the ranks are $k \times 8$ and $(8-k)\times 8$ $(k < 8)$; $\mathbf{d}_1$ and $\mathbf{d}_2$ are given vectors.

Eq. (19) is a set of nonlinear partial differential equations with eight basic unknown variables, the difficulties are how to solve directly the equations. First, Newmark's stable finite equidifferent formulas [7] are used to find the derivatives with respect to time in Eqs. (11) – (18) for a time step length:

$$\ddot{u}^{t+\Delta t} = \frac{u^{t+\Delta t} - u^t}{\beta(\Delta t)^2} - \left[\frac{\dot{u}^t}{\Delta t} + \ddot{u}^t\left(0,5-\beta\right)\right]\frac{1}{\beta}; \quad \dot{u}^{t+\Delta t} = \dot{u}^t + 0,5\Delta t\,(\ddot{u}^t + \ddot{u}^{t+\Delta t}), \tag{21a, b}$$

where Δt is the time difference step length; β is the parameter of the scheme, when $\beta = 0,25,$ Newmark's arithmetic operators for linear dynamic system are unconditionally stable [22].

After differencing, Eqs. (11) – (18) can be expressed as

$$\frac{\mathrm{d}\mathbf{N}}{\mathrm{d}s} = \mathbf{F}(s, \mathbf{N}) \quad (s_0 \le s \le s_N); \tag{22}$$

$$D_1\mathbf{N}(s_0) = \mathbf{d}_1; \quad D_2\mathbf{N}(s_N) = \mathbf{d}_2. \tag{23a, b}$$

In order to solve the nonlinear problem described by Eq. (22), with an iterative method, thus, nonlinear problems can be turned into a series of linear problems. Taken iterative equations are [7]

$$\frac{d\,\mathbf{N}^{(k+1)}}{ds} = \mathbf{F}(s, \mathbf{N}^{(k)}) + \mathbf{\Gamma}(s, \mathbf{N}^{(k)})(\mathbf{N}^{(k+1)} - \mathbf{N}^{(k)}); \tag{24}$$

$$D_1\mathbf{N}^{(k+1)}(s_0) = \mathbf{d}_1; \quad D_2\mathbf{N}^{(k+1)}(s_N) = \mathbf{d}_2 \quad (k = 0, 1, 2\ldots), \tag{25a, b}$$

where $\mathbf{\Gamma}(s, \mathbf{N}^{(k)})$ is Jacobi's matrix.

By using Eqs. (11) – (18), we have the linear iterative equations:

$$\frac{du^{(k+1)}}{ds} =$$

$$= \frac{1-\nu^2}{Eh} N_s^{(k+1)} + \frac{1}{2}(\theta_s^{(k)})^2 - \theta_s^{(k+1)}\theta_s^{(k)} - \frac{\nu\sin\varphi}{r} w^{(k+1)} - \frac{\nu\cos\varphi}{r} u^{(k+1)} + (1+\nu)\,\varepsilon_T^{(k+1)}; \tag{26}$$

$$\frac{dw^{(k+1)}}{ds} = -\theta_s^{(k+1)}; \tag{27}$$

$$\frac{d\,\theta_s^{(k+1)}}{ds} = \frac{12\,(1-\nu^2)}{Eh^3} M_s^{(k+1)} - \frac{\nu\cos\varphi}{r}\,\theta_s^{(k+1)} + (1+\nu)\,\kappa_T^{(k+1)}; \tag{28}$$

$$\frac{\mathrm{d}N_s^{(k+1)}}{\mathrm{d}s} = \frac{\cos\varphi}{r}\left[(\nu-1)N_s^{(k+1)} - Eh\varepsilon_T^{(k+1)} + Eh\left(\frac{\cos\varphi}{r}u^{(k+1)} + \frac{\sin\varphi}{r}w^{(k+1)}\right)\right] -$$

$$-(F_s + \rho f_s)^{(k+1)} + \rho h\frac{\partial^2 u^{(k+1)}}{\partial t^2}; \tag{29}$$

$$\frac{dQ_s^{(k+1)}}{ds} = -\frac{\cos\varphi}{r}Q_s^{(k+1)} + \frac{\sin\varphi}{r}\left[\nu N_s^{(k+1)} - Eh\varepsilon_T^{(k+1)} + Eh\left(\frac{\cos\varphi}{r}u^{(k+1)} + \frac{\sin\varphi}{r}w^{(k+1)}\right)\right] -$$

$$-(F_\zeta + \rho f_\zeta)^{(k+1)} + \rho h\frac{\partial^2 w^{(k+1)}}{\partial t^2}; \tag{30}$$

$$\frac{\mathrm{d}M_s^{(k+1)}}{\mathrm{d}s} =$$

$$= \frac{\cos\varphi}{r}\left[(\nu-1)M_s^{(k+1)} + \frac{Eh^3}{12}\left(\frac{\cos\varphi}{r}\theta_s^{(k+1)} - \kappa_T^{(k+1)}\right)\right] + N_s^{(k+1)}\theta_s^{(k)} + N_s^{(k)}\theta_s^{(k+1)} - N_s^{(k)}\theta_s^{(k)} -$$

$$-\frac{\nu\sin\varphi}{r}\left[M_s^{(k+1)}\theta_s^{(k)} + M_s^{(k)}\theta_s^{(k+1)} - M_s^{(k)}\theta_s^{(k)}\right] - \frac{Eh^3}{12}\cdot\frac{\sin\varphi\cos\varphi}{r^2}\left[2\theta_s^{(k+1)}\theta_s^{(k)} - (\theta_s^{(k)})^2\right] +$$

$$+\frac{Eh^3}{12}\cdot\frac{\sin\varphi}{r}\left[\kappa_T^{(k+1)}\theta_s^{(k)} + \kappa_T^{(k)}\theta_s^{(k+1)} - \kappa_T^{(k)}\theta_s^{(k)}\right] + Q_s^{(k+1)} + \frac{\rho h^3}{12}\cdot\frac{\partial^2\theta_s^{(k+1)}}{\partial t^2}; \tag{31}$$

$$\frac{dB_\zeta^{(k+1)}}{ds} = -\sigma\mu\left[E_\theta^{(k+1)} + \frac{1}{2}(B_s^+ + B_s^-)\frac{\partial w^{(k+1)}}{\partial t} - B_\zeta^{(k)}\frac{\partial u^{(k+1)}}{\partial t} - B_\zeta^{(k+1)}\frac{\partial u^{(k)}}{\partial t} + B_\zeta^{(k)}\frac{\partial u^{(k)}}{\partial t}\right] +$$

$$+\frac{B_s^+ - B_s^-}{rh}; \tag{32}$$

$$\frac{dE_\theta^{(k+1)}}{ds} = -\frac{\partial B_\zeta^{(k+1)}}{\partial t} - \frac{\cos\varphi}{r}E_\theta^{(k+1)}. \tag{33}$$

The Lorentz forces in Eqs. (26) – (33) can be written as

$$\rho f_s^{(k+1)} = hJ_{\theta cl}B_\zeta^{(k+1)} + \sigma h(E_\theta^{(k+1)}B_\zeta^{(k)} + E_\theta^{(k)}B_\zeta^{(k+1)} - E_\theta^{(k)}B_\zeta^{(k)}) +$$

$$+\frac{1}{2}\sigma h\,(B_s^+ + B_s^-)\left(B_\zeta^{(k)}\frac{\partial w^{(k+1)}}{\partial t} + B_\zeta^{(k+1)}\frac{\partial w^{(k)}}{\partial t} - B_\zeta^{(k)}\frac{\partial w^{(k)}}{\partial t}\right) - \tag{34}$$

$$-\sigma h\left[(B_\zeta^{(k)})^2\frac{\partial u^{(k+1)}}{\partial t} + 2B_\zeta^{(k)}B_\zeta^{(k+1)}\frac{\partial u^{(k)}}{\partial t} - 2(B_\zeta^{(k)})^2\frac{\partial u^{(k)}}{\partial t}\right];$$

$$\rho f_\zeta^{(k+1)} = -\frac{1}{2}hJ_{\theta cl}(B_s^+ + B_s^-) - \sigma h\left\{\left[\frac{1}{12}(B_s^+ - B_s^-)^2 + \frac{1}{4}(B_s^+ + B_s^-)^2\right]\frac{\partial w^{(k+1)}}{\partial t} +\right.$$

$$+\frac{1}{2}(B_s^+ + B_s^-)E_\theta^{(k+1)} - \frac{1}{2}(B_s^+ + B_s^-)\left(B_\zeta^{(k)} \frac{\partial u^{(k+1)}}{\partial t} + B_\zeta^{(k+1)} \frac{\partial u^{(k)}}{\partial t} - B_\zeta^{(k)} \frac{\partial u^{(k)}}{\partial t} \right) - \quad (35)$$

$$-\frac{h}{12}(B_s^+ - B_s^-)\left(B_\zeta^{(k)} \frac{\partial \theta_s^{(k+1)}}{\partial t} + B_\zeta^{(k+1)} \frac{\partial \theta_s^{(k)}}{\partial t} - B_\zeta^{(k)} \frac{\partial \theta_s^{(k)}}{\partial t} \right) \Bigg\}.$$

4. Electromagnetic Temperature Effect.

By using the electrodynamics equations and generalized Ohm's law, and considering the side electric current J_{scl} and $J_{\theta cl}$, we obtain [7]:

$$J_s = J_{scl} + \sigma E_s + \sigma\left(\frac{\partial v}{\partial t} B_\zeta - \frac{\partial w}{\partial t} B_\theta \right); \quad J_\theta = J_{\theta cl} + \sigma E_\theta + \sigma\left(\frac{\partial w}{\partial t} B_s - \frac{\partial u}{\partial t} B_\zeta \right). \quad (36a, b)$$

Because of Joule's heat effect in the electromagnetic field, the heat source is certainly produced in the current-carrying conical frustum. Considering the thin shell discussed and the electromagnetic field of low frequency, so the skin effect is not obvious. We can consider approximately that the distribution of the electric current density is symmetrical in the thin shell. Thus, the heat source power can be expressed as [23]

$$Q = 0,86\frac{J^2}{\sigma} = 0,86\frac{J_s^2 + J_\theta^2}{\sigma}. \quad (37)$$

Without considering external heat source and the local temperature effect of the conical frustum ends, considering only the heat exchange between the outer, inner surfaces of the conical frustum and the exterior. We consider that the distribution of the heat source power density along the thickness of the thin shell is symmetrical. At the neutral surface $\zeta = 0$, the heat flux $q = 0$; at the outer surface $\zeta = h/2$, the heat flux $q = Q\,h/2$, and $T = T_w$.

Thus, the equation of the temperature distribution in the ζ-direction can be written as

$$T = T_f + \frac{Q\,h^2}{8\lambda_T}\left[1 + \frac{4\lambda_T}{h\alpha_F} - 4\left(\frac{\zeta}{h} \right)^2 \right] - \frac{\rho hc}{2\alpha_F}\dot{T}_w, \quad (38)$$

where λ_T is the heat exchange coefficient of the material; c is the specific heat capacity of the material; α_F is the surface heat exchange coefficient of the material; T_w is the surface temperature of the thin shell; T_f is the temperature of the medium bordering upon the thin shell; $\dot{T}_w$ is the change rate of the surface temperature.

Using Eqs. (10), (36), (37), and (38), we obtain:

$$\varepsilon_T^{(k+1)} =$$

$$= \frac{43\alpha_T h^2}{400\sigma\lambda_T}\Bigg\{ J_{\theta cl}^2 + \sigma^2\left[2E_\theta^{(k+1)}E_\theta^{(k)} - (E_\theta^{(k)})^2 \right] + \sigma^2\Bigg[B_s^2\left(2\frac{\partial w^{(k+1)}}{\partial t}\cdot\frac{\partial w^{(k)}}{\partial t} - \left(\frac{\partial w^{(k)}}{\partial t} \right)^2 \right) +$$

$$+ 2\frac{\partial u^{(k+1)}}{\partial t}\cdot\frac{\partial u^{(k)}}{\partial t}(B_\zeta^{(k)})^2 + 2\left(\frac{\partial u^{(k)}}{\partial t} \right)^2 B_\zeta^{(k+1)}B_\zeta^{(k)} - 3\left(\frac{\partial u^{(k)}}{\partial t} \right)^2 (B_\zeta^{(k)})^2 -$$

$$- 2B_s\left(\frac{\partial w^{(k+1)}}{\partial t}\cdot\frac{\partial u^{(k)}}{\partial t}B_\zeta^{(k)} + \frac{\partial w^{(k)}}{\partial t}\cdot\frac{\partial u^{(k+1)}}{\partial t}B_\zeta^{(k)} + \frac{\partial w^{(k)}}{\partial t}\cdot\frac{\partial u^{(k)}}{\partial t}B_\zeta^{(k+1)} - 2\frac{\partial w^{(k)}}{\partial t}\cdot\frac{\partial u^{(k)}}{\partial t}B_\zeta^{(k)} \right)\Bigg] +$$

$$+2J_{\theta cl}\sigma E_{\theta}^{(k+1)}+2J_{\theta cl}\sigma\left[\frac{\partial w^{(k+1)}}{\partial t}B_s-\left(\frac{\partial u^{(k+1)}}{\partial t}B_{\zeta}^{(k)}+\frac{\partial u^{(k)}}{\partial t}B_{\zeta}^{(k+1)}-\frac{\partial u^{(k)}}{\partial t}B_{\zeta}^{(k)}\right)\right]+$$

$$+2\sigma^2\left[B_s\left(E_{\theta}^{(k+1)}\frac{\partial w^{(k)}}{\partial t}+E_{\theta}^{(k)}\frac{\partial w^{(k+1)}}{\partial t}-E_{\theta}^{(k)}\frac{\partial w^{(k)}}{\partial t}\right)-\right. \tag{39}$$

$$\left.-\left(E_{\theta}^{(k+1)}B_{\zeta}^{(k)}\frac{\partial u^{(k)}}{\partial t}+E_{\theta}^{(k)}B_{\zeta}^{(k+1)}\frac{\partial u^{(k)}}{\partial t}+E_{\theta}^{(k)}B_{\zeta}^{(k)}\frac{\partial u^{(k+1)}}{\partial t}-2E_{\theta}^{(k)}B_{\zeta}^{(k)}\frac{\partial u^{(k)}}{\partial t}\right)\right]\Bigg\}\times$$

$$\times\left(\frac{4\lambda_T}{h\alpha_F}+\frac{2}{3}\right)-\frac{\alpha_T\rho hc}{2\alpha_F}\dot{T}_w^{(k+1)};$$

$$\kappa_T^{(k+1)}=0\,. \tag{40}$$

The $\varepsilon_T^{(k+1)}$ and $\kappa_T^{(k+1)}$ are substituted in Eqs. (26) – (33), the thermal-magnetic-elastic coupling equations for the thin conical frustum shell are obtained. All unknown variables can be found by the discrete-orthogonalization method.

5. Numerical Results and Discussion.

Fig. 1 shows a thin cantilever conical frustum shell made of aluminum in a magnetic field $\mathbf{B}=\{B_s,0,0\}$. It bears the mechanical load $\mathbf{F}=\{0,0,F_{\zeta}\}$, alternating electric current that the density is $\mathbf{J_{cl}}=\{0,J_{\theta cl},0\}$ is exteriorly imported the shell. Let $E=71\,\text{GPa}$; $\nu=0,34$; $\rho=2670\,\text{kg}/\text{m}^3$; $\sigma=3,63\times10^7(\Omega\cdot\text{m})^{-1}$; $\mu=1,256\times10^{-6}\,\text{H/m}$; $c=934\,\text{J}/(\text{kg}\cdot{}^\circ\text{C})$; $\lambda_T=237\,\text{W}/(\text{m}\cdot{}^\circ\text{C})$; $\alpha_F=235\,\text{W}/(\text{m}^2\cdot{}^\circ\text{C})$; $\alpha_T=2,35\times10^{-5}\,{}^\circ\text{C}^{-1}$; $J_{\theta cl}=J_{\theta}\sin\omega t\,\text{A}/\text{m}^2$; $\omega=\pi\times10^2\,\text{sec}^{-1}$; $F_{\zeta}=F_0+(s-s_0)\tan\alpha\,\text{N}/\text{m}^2$; $F_0=-100$; $\alpha=\pi/12$; $h=2\times10^{-3}\,\text{m}$; $r_0=0,25\,\text{m}$; $\varphi=\pi/4$; $s_0=0,35\,\text{m}$; $s_N=0,85\,\text{m}$.

The boundary conditions are

$$s=s_0:\ u=0\,,\ w=0\,,\ \theta_s=0\,,\ B_{\zeta}=0,1\sin\omega t\,\text{T}; \tag{41a-d}$$

$$s=s_N:\ N_s=0\,,\ Q_s=0\,,\ M_s=0\,,\ B_{\zeta}=0. \tag{42a-d}$$

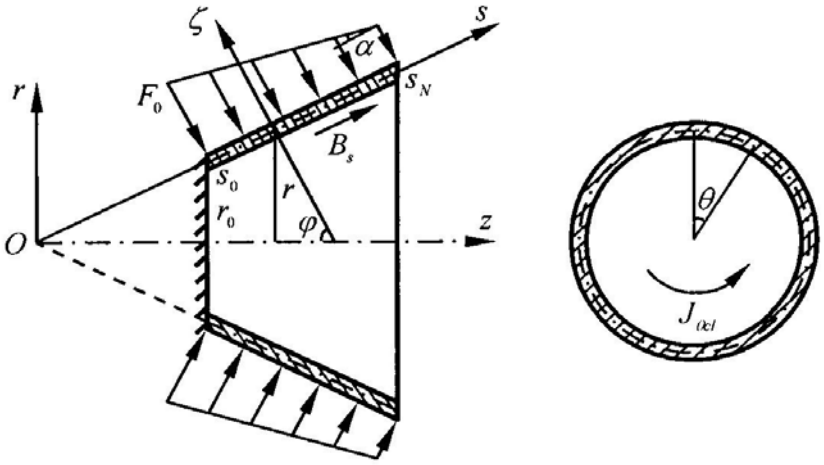

Fig. 1. A thin cantilever conical frustum shell in a magnetic field.

The initial conditions are

$$\mathbf{N}(s,t)\big|_{t=0} = 0\,;\;\; \dot{u}(s,t)\big|_{t=0} = \dot{w}(s,t)\big|_{t=0} = \dot{\theta}_s(s,t)\big|_{t=0} = \dot{B}_\zeta(s,t)\big|_{t=0} = 0; \qquad \text{(43a-e)}$$

$$\ddot{u}(s,t)\big|_{t=0} = \ddot{w}(s,t)\big|_{t=0} = \ddot{\theta}_s(s,t)\big|_{t=0} = 0. \qquad \text{(44a-c)}$$

In order to acquire stabilizing computational process, mass coordinate $m = \rho s$ is taken. Programming Eqs. (26) – (33) and conducting computations for the known data and the boundary and initial conditions yield the eight basic unknown variables u, w, θ_s, N_s, Q_s, M_s, B_ζ, and E_θ. Then the relations and variation laws between the mechanical and electromagnetic variables can be determined by changing the relevant parameters.

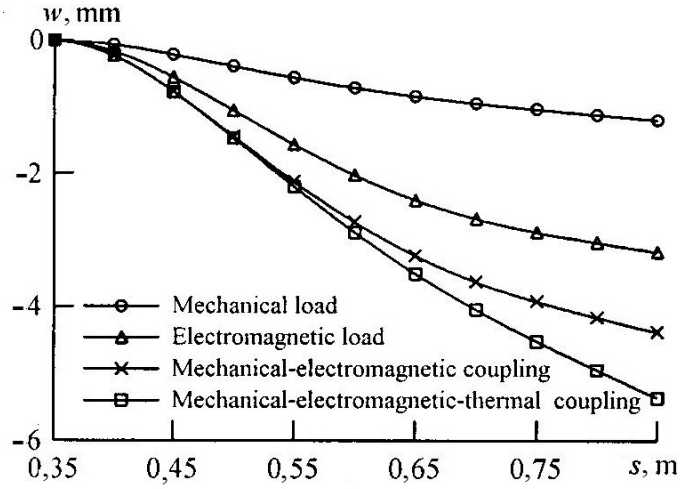

Fig. 2. Effects of the coupling action on the deflection in the thin conical frustum shell.

Fig. 2 shows the deflection distribution in the thin conical frustum shell for $J_\theta = 2\,\mathrm{MA/m^2}$, $B_s = 0{,}1\,\mathrm{T}$, and $t = 11\,\mathrm{msec}$, the mechanical load being the same as above. According to Fig. 2, the coupling action effect of different loads can be seen. Fig. 3 and fig. 4

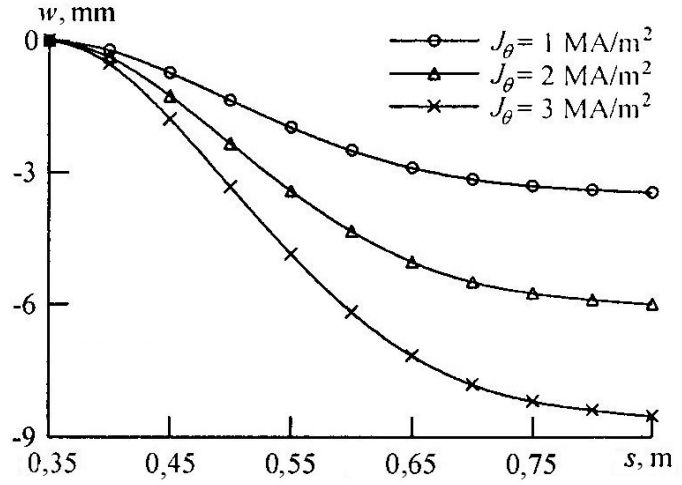

Fig. 3. Curves of the deflection distribution for $B_s = 0{,}2\,\mathrm{T}$, $t = 10\,\mathrm{msec}$, and different values of J_θ.

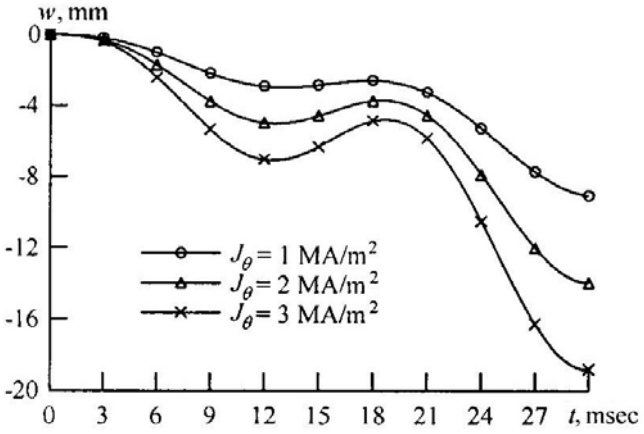

Fig. 4. The deflection at $s = 0,6\,\text{m}$ versus t for $B_s = 0,2\,\text{T}$ and different values of J_θ.

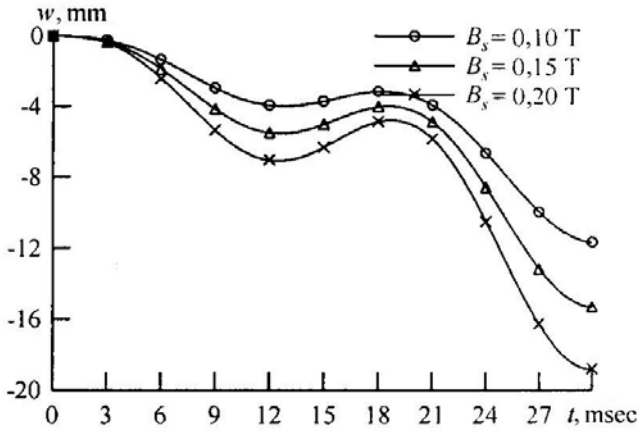

Fig. 5. The deflection at $s = 0,6\,\text{m}$ versus t for $J_\theta = 3\,\text{MA/m}^2$ and different values of B_s.

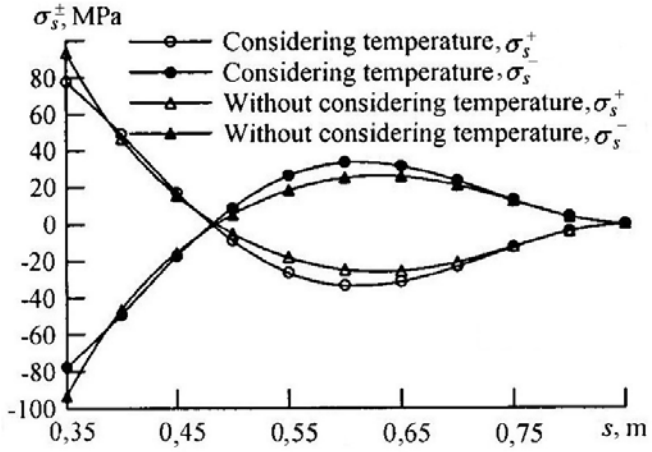

Fig. 6. Effects of the temperature on the stress in the thin conical frustum shell.

show the deflection distribution in the thin conical frustum shell ($t = 10\,\text{msec}$) and the variation of the deflection at $s = 0,6\,\text{m}$ with time for $B_s = 0,2\,\text{T}$ and different electric current density, respectively. The deflection in the thin shell increases with increase in the electric current density. Fig. 5 shows the variation of the deflection at $s = 0,6\,\text{m}$ with time for $J_\theta = 3\,\text{MA/m}^2$ and different magnetic induction intensity. Initially, the deflection varies a little with increase in the magnetic induction intensity. As time goes on, the deflection rapidly increases with the magnetic induction intensity. Fig. 6 shows the distribution of the normal stress σ_s^- and σ_s^+ in the s-direction on the inner and outer surfaces of the shell for $J_\theta = 5\,\text{MA/m}^2$, $B_s = 0,3\,\text{T}$, and $t = 9$ msec. According to Fig. 6, the effect of the temperature on the stress of the thin shell is relatively remarkable. Fig. 7 shows the distribution of the normal stresses σ_s^- and σ_s^+ in the s-direction on the inner and outer surfaces of the shell for $B_s = 0,2\,\text{T}$, $t = 10\,\text{msec}$, and different electric current density. Fig 8 shows the distribution

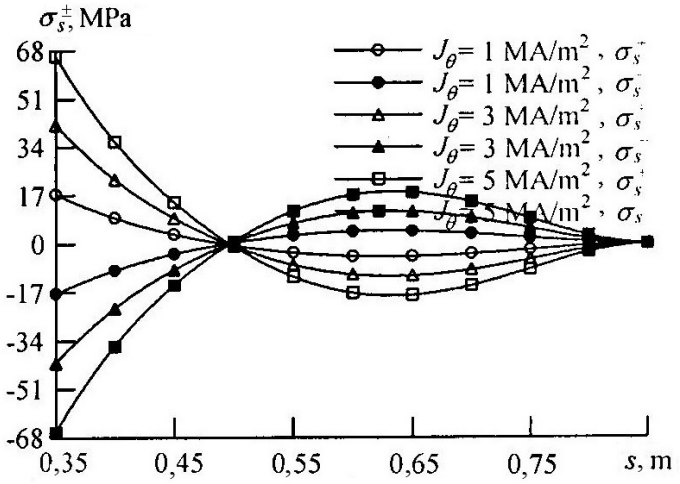

Fig. 7. Curves of the stresses σ_s^- and σ_s^+ distribution for $B_s = 0,2\,\text{T}$, $t = 10\,\text{msec}$, and different values of J_θ.

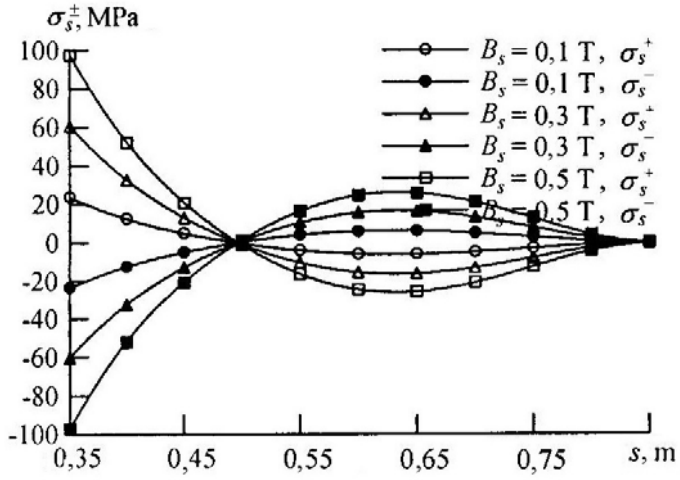

Fig. 8. Curves of the stresses σ_s^- and σ_s^+ distribution for $J_\theta = 3\,\text{MA/m}^2$, $t = 10\,\text{msec}$, and different values of B_s.

of the normal stresses σ_s^- and σ_s^+ in the s-direction on the inner and outer surfaces of the shell for $J_\theta = 3\,\mathrm{MA/m^2}$, $t = 10\,\mathrm{msec}$, and different magnetic induction intensity. Fig. 9 shows the variation of the normal stress σ_s^+ in the s-direction on the outer surface at the fixed end $(s = 0{,}35\,\mathrm{m})$ with time for $J_\theta = 3\,\mathrm{MA/m^2}$ and different magnetic induction intensity. Initially, the stress varies a little with increase in the magnetic induction intensity. As time goes on, the stress rapidly increases with the magnetic induction intensity, peaking generally at $t = 29\,\mathrm{msec}$.

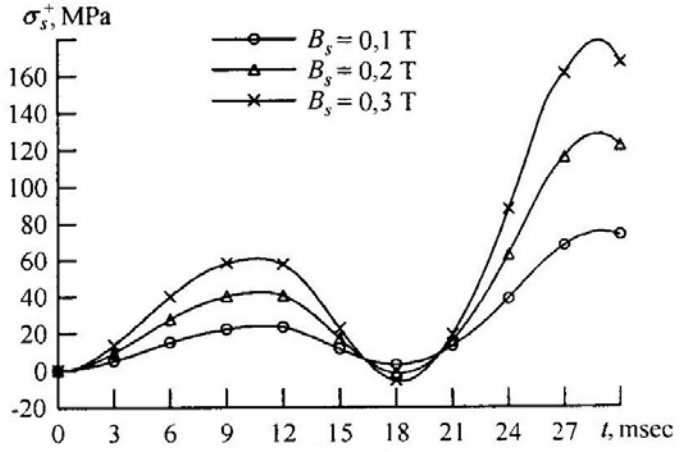

Fig. 9. The normal stress σ_s^+ at the fixed end $(s = 0{,}35\,\mathrm{m})$ versus t for $J_\theta = 3\,\mathrm{MA/m^2}$ and different values of B_s.

Fig. 10 shows the distribution of the normal stress σ_s^- and σ_s^+ in the s-direction on the inner and outer surfaces of the shell for $J_\theta = 3\,\mathrm{MA/m^2}$, $B_s = 0{,}2\,\mathrm{T}$, $t = 10\,\mathrm{msec}$, and different thickness of the shell. According to Fig. 10, the effect of the thickness on the stress of the thin shell is very remarkable.

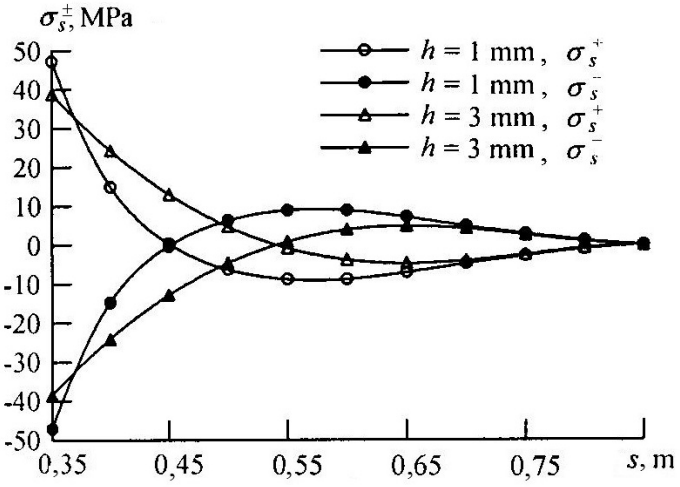

Fig. 10. Curves of the stresses σ_s^- and σ_s^+ distribution for $J_\theta = 3\,\mathrm{MA/m^2}$, $B_s = 0.2\,\mathrm{T}$, $t = 10\,\mathrm{msec}$, and different values of h.

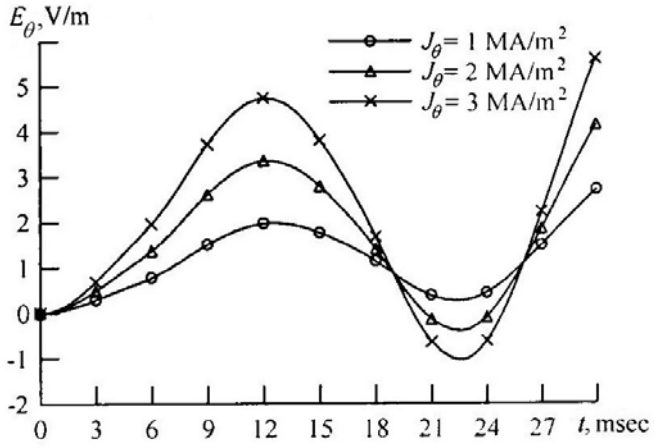

Fig. 11. The electric field intensity at the free end $(s = 0,85\,\text{m})$ versus t for $B_s = 0,2\,\text{T}$ and different values of J_θ.

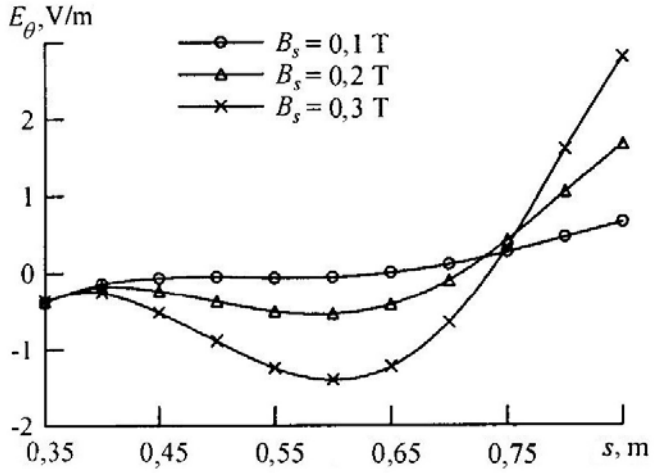

Fig. 12. Curves of the electric field intensity distribution for $J_\theta = 3\,\text{MA/m}^2$, $t = 18\,\text{msec}$, and different values of B_s.

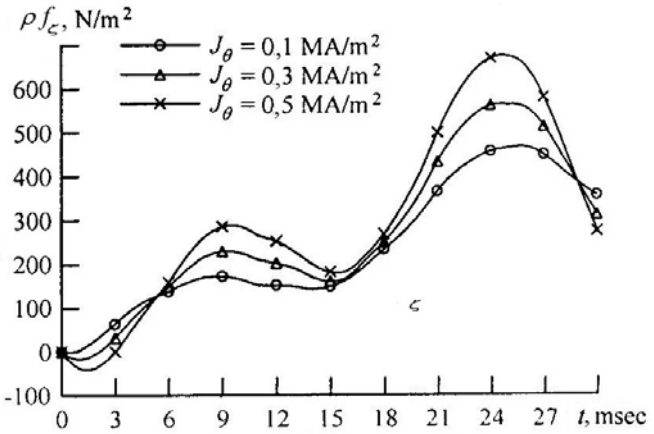

Fig. 13. The Lorentz force ρf_ζ at $s = 0,6\,\text{m}$ versus t for $B_s = 0,2\,\text{T}$ and different values of J_θ.

Fig. 11 shows the variation of the electric field intensity E_θ at the free end $(s = 0,85\,\text{m})$ with time for $B_s = 0,2\,\text{T}$ and different electric current density. Initially, the value of the E_θ is small, and the E_θ varies a little with increase in the electric current density. As time goes on, the E_θ rapidly increases with the electric current density and changing tempestuous. It predicates that coupling effect is increasingly stronger. Fig. 12 shows the distribution of the electric field intensity in the thin conical frustum shell for $J_\theta = 3\,\text{MA/m}^2$, $t = 18\,\text{msec}$, and different magnetic induction intensity. According to Fig. 12, the distribution of the electric field intensity in the thin shell is asymmetric. The electric field intensity varies tempestuously with increase in the magnetic induction intensity. Fig. 13 shows the variation of the Lorentz force ρf_ζ at $s = 0,6\,\text{m}$ with time for $B_s = 0,2\,\text{T}$ and different electric current density. According to Fig. 13, as time goes on, the Lorentz force rapidly increases, peaking generally at $t = 25\,\text{msec}$. The Lorentz force varies tempestuously with increase in the electric current density. Fig. 14 shows the temperature distribution in the thin conical frustum

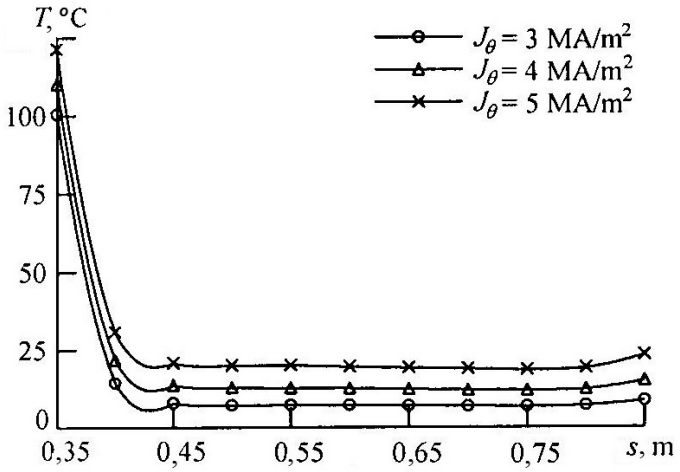

Fig. 14. Curves of the temperature distribution for $B_s = 0,2\,\text{T}$, $t = 19\,\text{msec}$, and different values of J_θ.

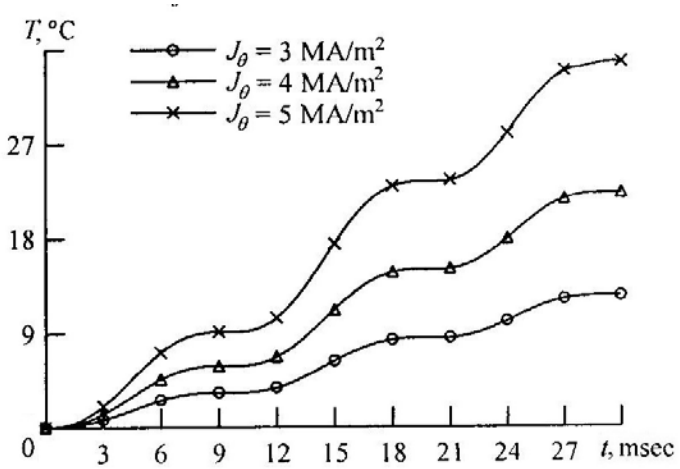

Fig. 15. The temperature at the free end $(s = 0,85\,\text{m})$ versus t for $B_s = 0,2\,\text{T}$ and different values of J_θ.

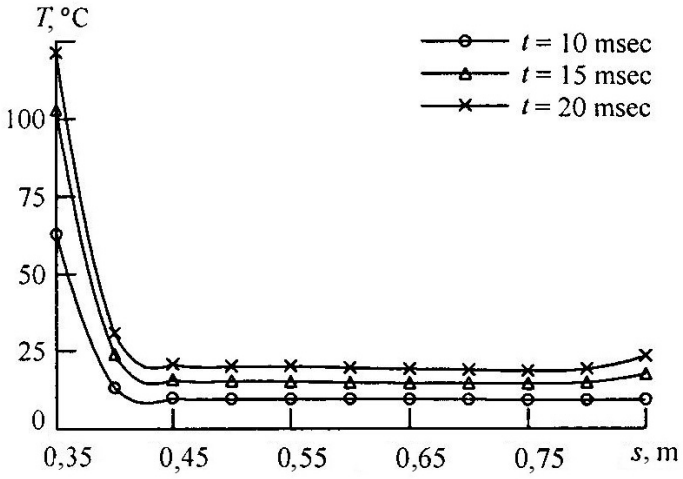

Fig. 16. Curves of the temperature distribution for $J_\theta = 5\,\text{MA/m}^2$, $B_s = 0,2\,\text{T}$, , and different moment.

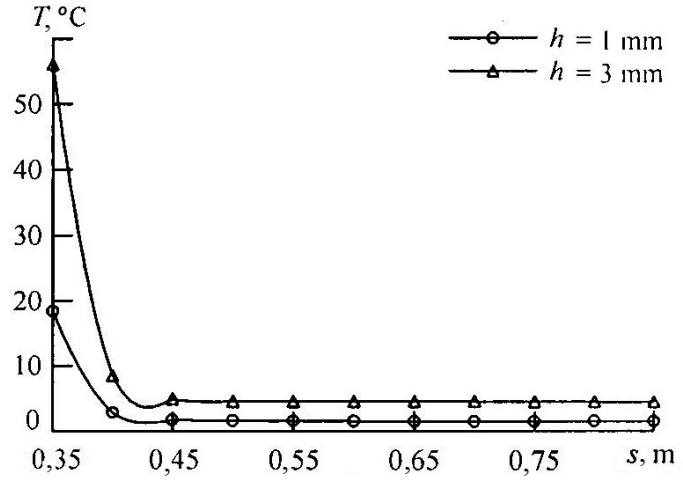

Fig. 17. Curves of the temperature distribution for $J_\theta = 3\,\text{MA/m}^2$, $B_s = 0,2\,\text{T}$, $t = 7\,\text{msec}$, and different values of h.

shell for $B_s = 0,2\,\text{T}$, $t = 19\,\text{msec}$, and different electric current density. According to Fig. 14, the value of the temperature at the fixed end $(s = 0,35\,\text{m})$ is the highest. Fig. 15 shows the variation of the temperature at the free end $(s = 0,85\,\text{m})$ with time for $B_s = 0,2\,\text{T}$ and different electric current density. Initially, the temperature varies a little with increase in the electric current density. As time goes on, the temperature rapidly increases with the electric current density. The results show that the temperature in the thin conical frustum shell can be controlled by changing the electric current density. Fig. 16 shows the temperature distribution in the thin conical frustum shell for $J_\theta = 5\,\text{MA/m}^2$, $B_s = 0,2\,\text{T}$, and different moment. Fig. 17 shows the temperature distribution in the thin conical frustum shell for $J_\theta = 3\,\text{MA/m}^2$, $B_s = 0,2\,\text{T}$, $t = 7\,\text{msec}$, and different thickness of the shell. According to Fig. 17, the effect of the thickness on the temperature of the thin shell is very remarkable.

6. Conclusions.

A thermal-magnetic-elastic problem for a thin current-carrying conical frustum shell in a magnetic field is studied. Using Newmark's stable finite equidifferent formulas and the quasi-linearization method, we have reduced nonlinear partial differential equations with eight basic unknown variables to normal Cauchy form linear ordinary differential equations, which can be solved by the discrete-orthogonalization method. Numerical solutions for magnetoelastic stresses and deformations in a thin conical frustum shell under the interaction of an electromagnetic field, a temperature field, and a mechanical field have been obtained. This lays the analytical foundation for practical applications of the thermal-magnetic-elastic problems on plates and shells. By the results, we now know that:

(1) the effect of an electromagnetic field of low intensity on the temperatures, deformations, and stresses of structures and components is weak, this effect becoming stronger with increase in the electromagnetic field intensity; it is shown that the thermal-magnetic-elastic analysis on the structures and components in an electromagnetic field is necessary and very important;

(2) the deformations and stresses in a thin conical frustum shell nonlinearly increase with the electric current density or magnetic induction intensity;

(3) the stress, strain, and temperature in plates and shells can be controlled by changing the electromagnetic and mechanical parameters;

(4) when the electric current density is large, the electromagnetic heat effect can not be ignored; when the electric current density is enough, the thermal stress will dominate.

Acknowledgements.

This research was partially supported by a grant from the National Natural Science Foundation of China, the Foundation of Key Laboratory of Nonlinear Continuum Mechanics, Institute of Mechanics of Chinese Academy of Sciences. The authors gratefully acknowledge these supports.

РЕЗЮМЕ. Вивчено термомагнітопружну задачу для тонкої конічної зрізаної оболонки, що проводить струм і перебуває у магнітному полі. Отримано методом заміни змінних нелінійні диференціальні рівняння нормального за Коші типу, які включають всього вісім невідомих змінних. За допомогою стійких скінченних формул Ньюмарка і методу квазілінеаризації нелінійні диференціальні рівняння з частинними похідними зведені до послідовності квазілінійних диференціальних рівнянь, які далі можуть розв'язуватися методом дискретної ортогоналізації. З розгляду теплового ефекту Джоуля в електромагнітному полі і рівняння теплової рівноваги визначено температурне поле в тонкій конічній зрізаній оболонці і інтегральні власні значення. На спеціальному прикладі проаналізовано зміну напружень, зміщень та температури зі зміною електромагнітних параметрів. Отримані результати матимуть теоретичне продовження в дослідженні поставленої задачі.

1. *Y.H. Pao, C.S. Yeh*, "A linear theory for soft ferromagnetic elastic bodies," Int. J. Eng. Sci., 11, No. 4, 415 – 436 (1973).
2. *S.A. Ambartsumyan, G.E. Bagdasaryan, M.V. Belubekyan.* Magnetoelasticity of Thin Shells and Plates [in Russian], Nauka, Moscow (1977).
3. *F.C. Moon.* Magneto-Solid Mechanics, John Wiley & Sons, New York (1984).
4. *A.A.F. Van de Ven, M.J.H. Couwenberg.* "Magneto-elastic stability of a superconducting ring in its own field," J. Eng. Math., 20, 251 – 270 (1986).
5. *A.T. Ulitko, L.V. Mol'chenko, V.F. Kovalchuk.* Magnetoelasticity under Dynamic Loading: A Workbook [in Ukrainian], Lybid', Kyiv (1994).
6. *L.V. Mol'chenko, Ya.M. Grigorenko.* Fundamental Theory of Magnetoelasticity for Elements of Thin Plates and Shells: A Textbook [in Ukrainian], Kyiv University (2010).
7. *L.V. Mol'chenko.* Nonlinear Magnetoelasticity of Thin Current-Carrying Shells [in Russian], Vyshcha Shkola, Kyiv (1989).
8. *L.V. Mol'chenko, I.I. Loos.* "Influence of the boundary conditions on the stress state of a flexible cylindrical shell of variable stiffness in a magnetic field," Int. Appl. Mech., 48, No. 1, 94 – 100 (2012).

9. *L.V. Mol'chenko, I.I. Loos.* "The stress state of a flexible orthotropic spherical shell subject to external current and mechanical force in a magnetic field," Int. Appl. Mech., 49, No. 5, 528 – 533 (2013).
10. *L.V. Mol'chenko, I.I. Loos, L.N. Fedorchenko.* "Influence of extraneous current on the stress state of an orthotropic ring plate with orthotropic conductivity," Int. Appl. Mech., 50, No. 6, 683 – 687 (2014).
11. *L.V. Mol'chenko, I.I. Loos.* "Axisymmetric magnetoelastic deformation of flexible orthotropic shells of revolution with orthotropic conductivity," Int. Appl. Mech., 51, No. 4, 434 – 442 (2015).
12. *L.V. Mol'chenko, I.I. Loos, L.N. Fedorchenko.* "Deformation of a flexible orthotropic spherical shell of variable stiffness in a magnetic field," Int. Appl. Mech., 52, No. 1, 56 – 61 (2016).
13. *Y.H. Bian.* "Analysis of nonlinear stresses and strains in a thin current-carrying elastic plate," Int. Appl. Mech., 51, No. 1, 108 – 120 (2015).
14. *X.J. Zheng, J.P. Zhang, Y.H. Zhou.* "Dynamic stability of a cantilever conductive plate in transverse impulsive magnetic field," Int. J. Solids Struct., 42, No. 8, 2417 – 2430 (2005).
15. *Z.M. Qin, L. Librescu, D. Hasanyan, et al.* "Magnetoelastic modeling of circular cylindrical shells immersed in a magnetic field," Int. J. Eng. Sci., 41, No. 17, 2005 – 2046 (2003).
16. *Z.M. Qin, D.J. Hasanyan, L.Librescu.* "Electroconductive cylindrical thin elastic shells carrying electric current and immersed in a magnetic field: Implications of the current-magnetic coupling on the shells' instability," Int. J. of Appl. Electromagnetics and Mechanics, 31, No. 2, 79 – 96 (2009).
17. *B. Pratiher.* "Non-linear response of a magneto-elastic translating beam with prismatic joint for higher resonance conditions," International Journal of Non-Linear Mechanics, 46, No. 5, 685 – 692 (2011).
18. *Y. Ootao, M. Ishihara.* "Transient thermoelastic analysis of a laminated hollow cylinder constructed of isotropic elastic and magneto-electro-thermoelastic materials," Advances in Materials Science and Applications, 2, No. 2, 48 – 59 (2013).
19. *Z.B. Kuang.* "An applied electro-magneto-elastic thin plate theory," Acta Mechanica, 225, No. 4, 1153 – 1166 (2014).
20. *S. Soni, N.K. Jain, P.V. Joshi.* "Analytical modeling for nonlinear vibration analysis of partially cracked thin magneto-electro-elastic plate coupled with fluid," Nonlinear Dynamics, 90, No. 1, 137 – 170 (2017).
21. *M. Mohammadimehr, R. Rostami.* "Bending and vibration analyses of a rotating sandwich cylindrical shell considering nanocomposite core and piezoelectric layers subjected to thermal and magnetic fields," Applied Mathematics and Mechanics, 39, No. 2, 219 – 240 (2018).
22. *R.E. Nickell.* "On the stability of approximation operators in problems of structural dynamics," Int. J. Solids Struct., 7, No. 3, 301 – 319 (1971).
23. *M.A. Mihaeev.* Basis of Heat Transfer [in Chinese], High Education Press, Beijing (1958).

From the Editorial Board: The article corresponds completely to submitted manuscript.

Поступила 17.04.2018 Утверждена в печать 05.11.2019
